LANGMUIR

pubs.acs.org/Langmuir Article

Surfactant Driven Marangoni Spreading in the Presence of Predeposited Insoluble Surfactant Monolayers

Madeline L. Sauleda, Henry C. W. Chu, Robert D. Tilton,* and Stephen Garoff*

Cite This: *Langmuir* 2021, 37, 3309−3320 Read Online

ACCESS | Metrics & More | Article Recommendations

ABSTRACT: When an insoluble surfactant is deposited on the surface of a thin fluid film, stresses induced by surface tension gradients drive Marangoni spreading across the subphase surface. The presence of a predeposited layer of an insoluble surfactant alters that spreading. In this study, the fluid film was aqueous, the predeposited insoluble surfactant was dipalmitoylphosphatidylcholine (DPPC), and the deposited insoluble surfactant was oleic acid. An optical density-based method was used to measure subphase surface distortion, called the Marangoni ridge, associated with propagation of the spreading front. The movement of the Marangoni ridge was correlated with movement of surface tracer particles that indicated both the boundary between the two surfactant layers and the surface fluid velocities. As the deposited oleic acid monolayer spread, it compressed the predeposited DPPC monolayer. During spreading, the surface tension gradient extended into the predeposited monolayer, which was compressed nonuniformly, from the deposited monolayer. The spreading was so rapid that the compressed predeposited surfactant could not have been in quasi-equilibrium states during the spreading. As the initial concentrations of the predeposited surfactant were increased, the shape of the Marangoni ridge deformed. When the initial concentration of the predeposited surfactant reached about 70 A^2/molecule, there was no longer a Marangoni ridge but rather a broadly distributed excess of fluid above the initial fluid height. The nonuniform compression of the annulus of the predeposited monolayer also caused tangential motion ahead of both the Marangoni ridge and the boundary between the two monolayers. Spreading ceased when the two monolayers reached the same final surface tension. The final area per molecule of the DPPC monolayer matched that expected from the equilibrium DPPC isotherm at the same final surface tension. Thus, at the end of spreading, there was a simple surface tension balance between the two distinct monolayers.

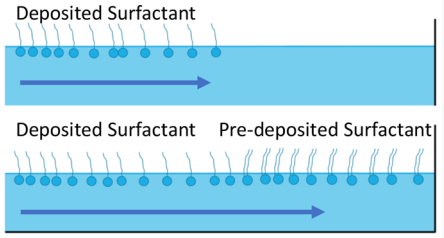

INTRODUCTION

Surface tension gradients arising from nonuniform deposition of surfactants on a liquid subphase surface cause Marangoni flows. The flow moves from regions of lower surface tension, where more surfactant is located, to regions of higher surface tension, where less or no surfactant is located. Marangoni flows arising from deposition of either a pure surfactant or a drop of a surfactant solution on a clean liquid subphase surface are well studied and occur in various technological settings (review articles may be found in refs. 1−4 and other references throughout this paper also discuss the subject). Surface tension gradients that drive Marangoni flows can lead to uneven coatings.[5,6] In oil spill remediation, deposition of surfactants can induce Marangoni flows that corral the spilled oil into a confined region where it can be pulled from the surface.[7]

The application which most directly motivates the present work in this paper is spreading on the liquid surface of the lung airways. Various pulmonary therapies, such as surfactant replacement therapy (SRT),[8] depend on Marangoni spreading.[9] There is also proposed pulmonary therapy intended to enhance postdeposition dispersal in aerosol drug delivery with surfactants.[10,11] Since endogenous pulmonary surfactant is present to differing degrees in different parts of the lung, exogenous surfactant added during treatment must induce spreading against the endogenous surfactant monolayer. The main lipid component of endogenous pulmonary surfactant is dipalmitoylphosphatidylcholine (DPPC). Since this lipid monolayer lowers the surface tension of the lung airways, its presence can hinder spreading of the administered surfactant.

In the case of no endogenous or predeposited surfactant, the subphase surface tension is uniform before an exogenous surfactant is deposited. Spreading is induced upon localized deposition of surfactant. A key controlling parameter is the surface tension difference between the initially bare subphase surface σ_o and the initial surface tension of the surfactant deposit σ_s This is usually expressed as a spreading parameter, $S = \sigma_o - \sigma_s$.[12] For $S > 0$, the deposited surfactant creates a surface tension gradient that drives Marangoni spreading

Received: November 20, 2020
Revised: March 2, 2021
Published: March 9, 2021

https://dx.doi.org/10.1021/acs.langmuir.0c03348
Langmuir 2021, 37, 3309−3320

outward on the subphase surface from the deposition site. The associated flow field has both tangential and normal components relative to the subphase surface. The sharp surface tension gradient between the advancing deposited surfactant and the clean subphase surface produces a sharp radial gradient in the tangential stress jump across the subphase surface. This abrupt variation in the tangential stress on the subphase surface deforms the subphase in the form of a "Marangoni ridge" in the vicinity of the surfactant front.[13] This shock-like structure then travels with the surfactant front along the subphase surface as time progresses.[1,2,14,15] Spreading ceases when the surfactant surface excess concentration is uniform across the surface and there is no longer a surface tension gradient.

If the subphase is a thin film on a solid support, the depression may cause dewetting. There can be gravity-driven recirculation flows present which recirculate fluid back to the center of deposition and prevent dewetting of the solid substrate below the subphase.[13,15] Recirculation flows are present when the ratio of gravity to surface tension forces, $G = \frac{H_o^2 \rho g}{S}$, is greater than one (where H_0 is the initial height of the subphase, g is the gravitational acceleration, and ρ is the density of the subphase).[13,15,16] For G less than one, recirculation flows are insufficient to prevent dewetting. Characteristics on the subphase surface are defined in Figure 1. The Marangoni ridge is trailed by a depression, and the

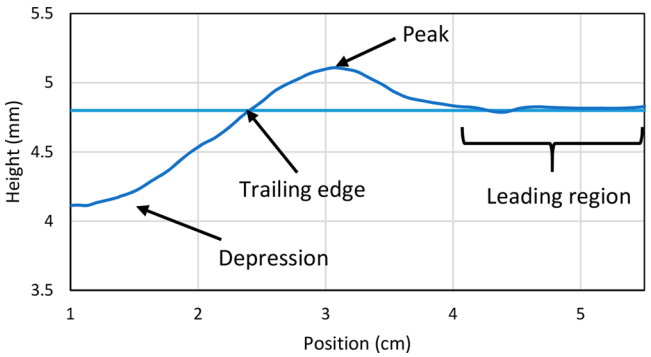

Figure 1. Four characteristic positions during spreading. The surface height profile is taken from experimental data and will be explained below.

trailing edge is defined as the location where the depression ends and the Marangoni ridge begins, i.e., where the subphase surface crosses the undisturbed subphase surface height. Ahead of the Marangoni ridge is the leading region, which is the region ahead of the Marangoni ridge where the surface height equals the initial, undisturbed fluid height.

A limited number of studies have examined spreading in the presence of a predeposited monolayer, most theoretically[8,13,17−23] and a few experimentally.[10,22−24] The previous theoretical and experimental work has found that the compression of the predeposited surfactant monolayer causes fluid motion for some finite distance ahead of the spreading deposited surfactant front.[17,18,22] The rate at which the outer boundary of this mobilized region of the predeposited surfactant moves was experimentally found to be dependent on the initial predeposited surfactant surface concentration,[22] with larger surface concentrations of predeposited surfactant causing faster rates of mobilization of the outer boundary within the predeposited monolayer. In contrast, the presence of a predeposited monolayer slows down the deposited surfactant front relative to its speed of propagation on an initially clean subphase surface.[17,22,23] As compression of the predeposited monolayer further decrease its surface tension, spreading halts when the two monolayers have the same surface tension.[13,17,18,22,24]

Another set of experiments with aerosolized DPPC vesicle suspensions spreading against predeposited DPPC monolayers found that spreading can occur even when the surfactant is the same for the deposited and predeposited surfactants and the predeposited monolayer is in the liquid condensed state.[10] This was shown to be due to the production of lower surface tensions by deposition of aerosolized vesicle suspensions.

In this paper, we experimentally measure how alteration of the surface stress conditions imposed by the presence of a predeposited monolayer alters the speed of the moving deposited surfactant front and the shape of the Marangoni ridge. We report the first detailed experimental observations of the change in the Marangoni ridge due to a predeposited surfactant. We used DPPC as the insoluble predeposited surfactant and oleic acid as the insoluble deposited surfactant. Observations of tracer particle motion within the predeposited monolayer allowed us to infer the nonuniformity of its compression during spreading. An optical density-based surface imaging technique revealed effects of the predeposited surfactant monolayer on the structure of the Marangoni ridge. Key observations include the nonuniformity of the predeposited monolayer compression ahead of the deposited surfactant front and a distortion of the ridge, including a subphase surface deformation ahead of the Marangoni ridge in the region of the predeposited monolayer. This deformation does not occur on an initially clean subphase surface. Ridge distortion increases in severity with increasing initial surface concentration of the predeposited surfactant monolayer ultimately eliminating the ridge.

MATERIALS AND METHODS

Materials. DPPC (Avanti Polar Lipids, >99%) and oleic acid (Sigma-Aldrich, >99%) were used as received. DPPC was dissolved in chloroform (Sigma-Aldrich, CHROMASOLV for HPLC >99.8%) at a concentration of 10 mg/mL to allow predeposition of the lipid on the subphase surface. The DPPC solution, the pure DPPC, and the oleic acid were stored at −16 °C between uses. Aqueous erythrosine dye (Sigma-Aldrich, >80%) solutions of concentration 0.025 g/L were made in ultrapurified water (Milli-Q Direct 8, 18 MΩ cm resistivity) and used as the subphase in experiments to support the use of the optical density-based subphase imaging technique.[16] Fluorescently tagged lipid, 1-palmitoyl-2-{12-[(7-nitro-2−1,3-benzoxadiazol-4-yl)-amino]dodecanoyl}-*sn*-glycero-3-phosphocholine (NBD-PC, Avanti Polar Lipids, >99%), was used to locate the DPPC on the subphase surface in some experiments. It was dissolved in chloroform, with 98 mol % DPPC and 2 mol % NBD-PC for spreading, with a total concentration of lipid (DPPC and NBD-PC) at 10 mg/mL. Talc (Sigma-Aldrich, < 10 μm) was used as a tracer of fluid movement.

Methods. Two experimental methods were used: one to track the radial movement of the subphase surface (the movement projected onto the plane of the undisturbed subphase surface) during the spreading event and the surface tension before and after spreading and the other to measure the vertical height deformation of the subphase surface during the spreading event. The radial velocity measured in the experiment was converted into tangential velocity along the subphase surface by taking into account the subphase deformation. Similarly, the vertical height deformation measured in the experiments was converted into a velocity normal to the subphase surface by taking into account the subphase deformation. The experiments were performed in glass Petri dishes with a diameter of

https://dx.doi.org/10.1021/acs.langmuir.0c03348
Langmuir 2021, 37, 3309−3320

14.5 cm. The undisturbed water subphase height before and after spreading was 4.8 mm. All experiments were conducted at room temperature, 22 ± 1 °C. In both methods, measured amounts of DPPC/chloroform solution were deposited, drop by drop, onto the water subphase using a microliter glass syringe. The initial area per DPPC molecule in the predeposited monolayer before spreading experiments was controlled by the total volume of the DPPC solution placed on the subphase. Table 1 summarizes the concentrations used.

Table 1. Tested Concentrations of Pre-Deposited Surfactant and Their Corresponding Initial Surface Tension, Initial Spreading Parameter, and the Marangoni Ridge Speed

DPPC concentration (Å^2/molecule)	initial surface tension (mN/m)	initial spreading parameter (mN/m)	speed (cm/s)
no predeposited DPPC	72.7	32	17.2 ± 2.7
200	71.7	31	16.3 ± 2.5
134	69	28.3	10.3 ± 1.2
80	65.8	25.1	8.7 ± 3.0
67	62.1	21.4	8.6 ± 3.7[a]

[a]For an initial DPPC concentration of 67 Å^2/molecule, the speed shown is the speed of the trailing edge, not the Marangoni ridge.

Surface tension was monitored with a Wilhelmy pin to ensure that ample time was given for chloroform evaporation between drops, so that the measured surface tension was solely due to the DPPC monolayer. Chloroform was deemed completely evaporated when the surface tension changed less than 0.2 mN/m over 15 s. A total of 1 min was sufficient for this to occur. The isotherm for DPPC made by this deposition method was used to specify the initial monolayer state before spreading. The isotherm obtained by this method matches well with other isotherms published in the literature, including the existence of the liquid expanded/liquid condensed coexistence regime.[10,25]

For both experimental methods, a 2 μL drop of oleic acid was gently deposited at the center of the Petri dish after the predeposited DPPC layer had relaxed. Detection of the location of predeposited DPPC on the subphase before and after spreading was performed in separate experiments using a fluorescence microscope (Nikon, AZ100, AZ-Plan Apo 4x (NA: 0.4/WD: 20 mm), AZ-TP DSC Tube 0.6x) and the NBD-PC fluorescently tagged lipid. Recording and analysis of these and all other microscope videos were conducted with NIS-Elements BR Analysis. Detection of the boundary between the two monolayers after spreading was performed using the microscope in fluorescence mode. The boundary can be seen in Figure 2.

Method 1: Surface Deformation. The time evolution of the surface deformation was measured using the previously described apparatus[16] shown schematically in Figure 3A. The camera (640 × 480px, 18px/cm, Q-SEE CCD Camera, QPSCDNV with 1/3″ 3.5−8 mm f1.4 Varifocal, Fixed Iris CCTV lens) was mounted directly above the sample, imaging through a 520−530 nm band-pass filter (Edmund Optics, CAT#65154). Movies of the spreading events were captured using Elgato video software, with a frame rate of 29 frames/s. The Petri dish rested on a light table to diffusely illuminate the entire subphase, with a box enclosing the apparatus to eliminate stray light. Instead of a pure water subphase, an erythrosine dye solution was used. The distortion of the surface was characterized by measuring the absorption of the light passing through the subphase as a function of position and time. Data for optical absorbance as a function of position and time was converted to a time series of spatial maps of subphase thickness via the Beer−Lambert relation for the dye solution. The benefit of our method, compared to past experiments using constructed-light method[23] is the direct measurement of the surface height rather than just the change of the slope on the surface. Data were azimuthally averaged and exponentially smoothed[26] to best locate the position of the Marangoni ridge and other important features of the surface deformation. We did not observe any fingering instabilities[2] or any other azimuthal variations during spreading in any experiments. Results are presented as plots of subphase thickness as a function of radial position. Calculation of the total subphase mass by integration of the thickness maps confirmed that the mapping satisfied the conservation of mass throughout the spreading experiment. Details of this method are described elsewhere.[16]

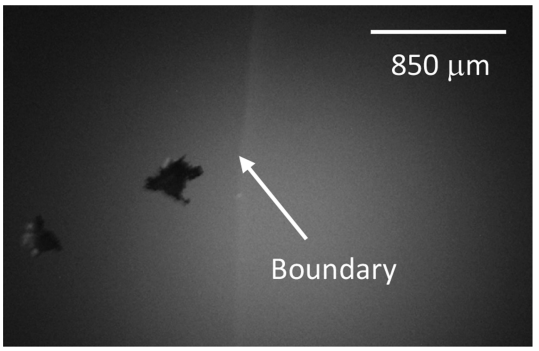

Figure 2. Fluorescence microscopy of 98% DPPC:2% NBD-PC and oleic acid. The final area per molecule of the lipid monolayer was 41.6 ± 3.4 Å^2. The oleic acid was deposited from the right. The boundary between the DPPC monolayer and the oleic acid is the bright line marked with an arrow. The talc solely resided on the DPPC monolayer: no talc was ever observed on the oleic acid side of the boundary. Image in the figure is shortly after spreading has occurred.

Only the time before the Marangoni ridge hit the wall of the Petri dish (the first 0.23 s of the spreading event) was analyzed to avoid the influence of fluid reflections from the Petri dish wall. The exponential smoothing parameter was adjusted so noise on the data was reduced but the surface shapes were not significantly distorted. All key features of the Marangoni ridge shape reported here were observed in the unsmoothed data as well. Smoothing was performed to aid in quantitative analysis. No reported features are the result of data smoothing. The temporal variation of the surface height provides a measure of the normal component of the fluid velocity at the surface. Given the maximum inclination of the surface found in the experiments reported here, which is equal to 2°, the apparent normal velocity measured from the surface displacement relative to the horizontal plane is at most 0.06% above the true surface normal velocity relative to the distorted surface. Such systematic errors have no impact on our conclusions. Therefore, we take these measurements of vertical velocity as representative of the fluid velocity normal to the surface. From the noise level on the surface height measurement, we estimate our detection limit on normal velocities to be ∼0.06 cm/s.

Method 2: Subphase Surface Radial Velocity. To track the radial movement of the subphase surface, talc was spread on the subphase using a sifter to disperse the particles with as little clumping as possible and at the lowest density that still allowed sampling motion over the entire surface. Microscope images of the particles on the subphase suggest they were not submerged in the subphase, both with and without the predeposited DPPC. We confirmed that the tracer particles tracked the fluid flow by calculating Stokes number for the talc particles:

$$Stk = \frac{\rho_p d_p^{\,2} u_0}{18 \mu l_0}$$

where u_0 is the speed of the particle during spreading, l_0 is the radius of the dish, ρ_p is the density of the particle, d_p is the diameter of a single particle, and μ is the density of the fluid subphase.[27] Stokes numbers below 1 indicate that the tracer particle is tracking the fluid flow. An estimate of the Stokes number of the tracer particles, even if they were completely submerged in water is $\sim 10^{-3}$. Despite the fact that the viscous coupling of the flow to the particle on the surface may

https://dx.doi.org/10.1021/acs.langmuir.0c03348
Langmuir 2021, 37, 3309−3320

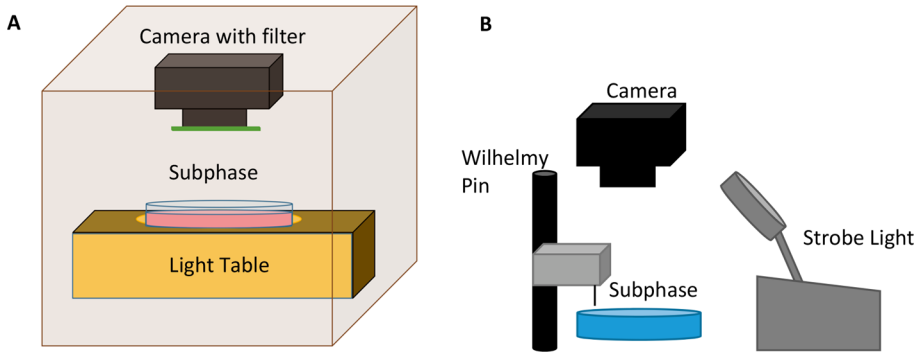

Figure 3. Schematics of the experimental apparatuses. Panel A: The dish containing the aqueous erythrosine dye solution subphase is illuminated via an opening in an opaque cover on a light table. Camera with bandpass filter records spreading experiments from above. Panel B: An aqueous subphase is illuminated at an oblique angle from the side. A Wilhelmy pin records the surface tension before and after the spreading while talc particles on the subphase track surface movement in the radial direction. A camera records the spreading from above. A strobe light operating at 70 Hz is used to superimpose multiple tracer positions onto one frame of a video.

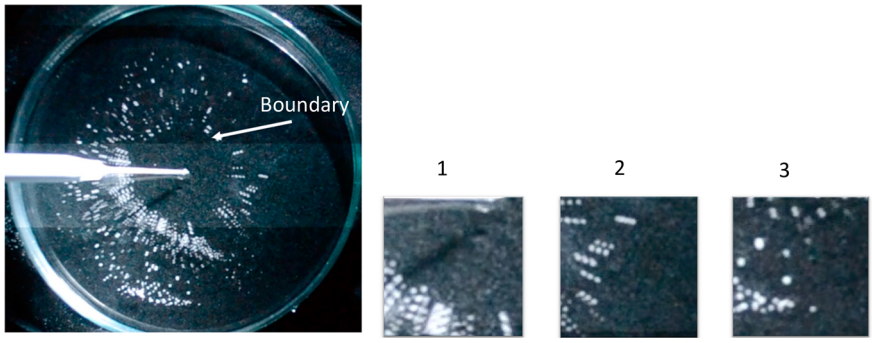

Figure 4. Image of one frame from an experiment initially with an area per DPPC molecule of 134 Å^2. The image shown here is at 50 ms after spreading began. The boundary between the deposited oleic acid and the predeposited DPPC monolayer is clearly indicated by the innermost tracer particles. The motion near the boundary is highlighted in subimage 1. Subimage 2 shows motion 1 cm away from the boundary. Subimage 3 shows lack of motion 3.5 cm way from the boundary. Subimages 1−3 were sharpened once using ImageJ.[28]

be reduced compared to their being completely submerged, we will assume that they track the surface velocity field.

For experiments where tracer particle movement was tracked in parallel with surface tension measurements, the apparatus shown in Figure 3b was used. The camera (640 × 424px, Nikon D3100, 24 fps with Nikon DX SWM VR Aspherical 0.28m-0.92 ft lens) was mounted on a tripod looking vertically down on the Petri dish. Rather than using a light table, the surface was illuminated obliquely with a strobe light, set at a frequency of 70 Hz to produce 2−3 particle images in a video frame (24 frames per second) for the fastest moving particles.

Figure 4 shows a typical image where the fastest moving particles were captured as three distinct images per frame. Particles that appear as one bright spot were moving slower than the detectable velocity in a single frame. Particles must have moved more than one particle diameter per frame to have produced multiple discretely detectable positions in one frame. Therefore, a particle must have a radial velocity of at least 200 μm/s to move detectably in one frame. This is only 0.2% of the typical velocities of the spreading surfactant front. Videos of the spreading were analyzed with ImageJ[28] (National Institutes of Health).

Given the maximum inclination of the surface found in the experiments reported here, the measured radial velocity is at most 0.06% below the fluid velocity tangential to the deformed subphase surface. As with normal velocities, such systematic errors have no impact on our conclusions, and we take the radial velocity measurements as representative of the tangential velocity along the surface. Given the detectability limit of the radial velocity described above, the detectability limit of the tangential velocity is also ∼0.2% of the typical spreading velocities in the spreading experiments.

The surface tension of the monolayer was measured before and after the spreading event using a Wilhelmy pin. The pin was located 1−2 cm from the edge of the dish, to avoid the effects of capillary rise at the edge of the dish while consistently remaining within the predeposited DPPC monolayer throughout the spreading event. The temporal resolution of the Wilhelmy pin apparatus did not allow surface tension measurements during spreading.

RESULTS

Boundary between the Deposited and Predeposited Surfactant. When there is no predeposited surfactant, the introduction of the deposited oleic acid monolayer induces a surface tension gradient which causes flow. We observed autophobing in the central region (as has been reported in the literature[29]), whereby spreading occurs as a monolayer is ejected from the deposited oleic acid drop, which stays at the center of deposition. At the end of all spreading (which occurs well after the times analyzed in our experiments), the excess oleic acid brakes up into several discrete lenses of liquid oleic acid. The lenses of oleic acid are in equilibrium with the oleic acid monolayer. Since this occurs after the compression of the predeposited surfactant, the formation of these lenses does not effect spreading. Previously in the literature, it has been seen that the predeposited tracer particles did not move until the Marangoni ridge reached the particles.[30] It is not known precisely where the particles are relative to the moving front of the deposited surfactant monolayer in this case.

https://dx.doi.org/10.1021/acs.langmuir.0c03348
Langmuir 2021, 37, 3309−3320

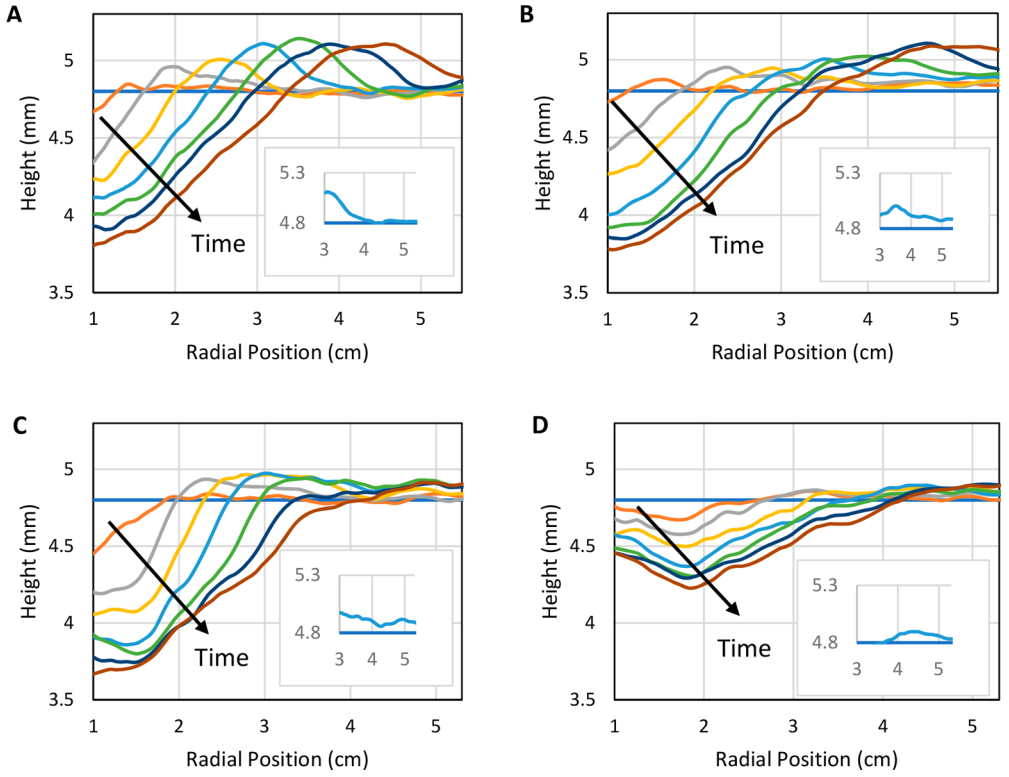

Figure 5. Temporal evolution of subphase height profiles during Marangoni spreading caused by deposition of a 2 μL oleic acid droplet. The earliest time (33 ms after deposition) is in orange, and the flow propagates outward as time progresses. Traces are recorded at 33 ms intervals up to 233 ms). Radial positions less than 1 cm are omitted to avoid image artifacts from the pipet used to deposit the oleic acid drop. The blue flat line is the undisturbed fluid height before spreading. Panel A: no predeposited surfactant. Panel B: predeposited DPPC initial average area of 200 Å^2/molecule. Panel C: 134 Å^2/molecule. Panel D: 67 Å^2/molecule. Insets show the typical traces at 133 ms at larger radial distances to highlight the leading region excess ahead of the Marangoni ridge. The edge of the dish is at 7.25 cm, but the analysis is not done past 5.5 cm due to height distortions caused by the dish edge.

In the case with predeposited surfactant, the talc was placed on the subphase surface after the predeposited DPPC but before oleic acid was deposited. Therefore, initially, the talc marks the region of subphase surface occupied by predeposited DPPC. Fluorescence imaging at the end of spreading showed that no talc particles resided within the deposited oleic acid region, and particles remained solely in the annulus of the predeposited DPPC/NBD-PC monolayer. Figure 4 shows a representative image for a DPPC monolayer initially at 134 Å^2/molecule, which is the liquid expanded regime. An inner region that had been swept free of tracer particles by the spreading oleic acid monolayer was surrounded by an outer region containing all of the talc particles. This behavior was independent of the initial phase of the DPPC predeposited layer. Therefore, we use the talc particles at the smallest radial position during spreading, the "innermost talc particles", as a marker of the boundary between the deposited oleic acid and the predeposited DPPC monolayers. This is consistent with the fluorescence microcopy result that was shown in Figure 2.

The talc particles within the outer annulus track the local motion of the DPPC monolayer. Using the area of the DPPC monolayer annulus between the innermost talc particles and the dish edge and the initial number of DPPC molecules predeposited, the average area per molecule of DPPC in the annulus can be calculated throughout the spreading event. Those results will be presented below. In addition, the boundary between the predeposited DPPC annulus and the area occupied by deposited oleic acid that is visible in the fluorescence images (see Figure 2) remained well-defined and did not become diffuse on the time scale of the experiments. This strongly suggests the predeposited DPPC and deposited oleic acid monolayers do not mix to a significant degree on the subsecond time scale of the spreading experiments, even though codeposited DPPC and oleic acid do show evidence of miscibility at equilibrium.[31−35] In addition, in our fluorescence imaging, we scanned the entire surface, and we did not see any evidence of the dark lines that are evidence of DPPC monolayer collapse as has been seen in Langmuir trough experiments.[36−39]

Spreading with No Predeposited Surfactant. The focus of this section is on spreading with no predeposited surfactant. Figures 5−8 report information for experiments conducted both with and without predeposited surfactant. Readers are referred to the appropriate figure panels for each type of experiment. The section labeled spreading with predeposited surfactant will focus on the experiments with predeposited surfactant and will refer to the appropriate figure panels.

Our results for the case of no predeposited surfactant agree with modeling done previously.[1,2,12,14,15] In this case, the spreading parameter S = 32 ± 1 mN/m. The water subphase was measured to have a surface tension of 72.7 ± 1 mN/m. The oleic acid monolayer was measured to have a surface tension of 40.7 ± 1 mN/m. The aspect ratio, ε, defined as the ratio of the subphase depth to the drop radius,[15] is ∼5. The Reynolds number, defined for this problem[15] as $Re = u_0R_0/\upsilon$,

https://dx.doi.org/10.1021/acs.langmuir.0c03348
Langmuir 2021, 37, 3309−3320

where u_0 is the speed of spreading, R_0 is the initial droplet radius, and μ is the kinematic viscosity of the subphase, is ~100. We also note that the dimensionless gravitational parameter $G \sim 10$ for our experiments. Since $G > 1$, recirculation flows are expected to be present and the experiments are well outside of the substrate dewetting regime during spreading. As expected, no dewetting was observed in any of our experiments.

Figure 5A shows the surface deformation following the deposition of the oleic acid drop on a subphase with no predeposited surfactant As predicted theoretically[12,15] and observed in previous experiments with other surfactants,[16] a depression develops near the deposition point as a ridge propagates outward in our data. The observed spreading indicates that a surface tension gradient exists in the oleic acid monolayer emitted from the deposited drop,[29] but it is not known whether the gradient occurs throughout the entire spreading monolayer or is highly concentrated at the leading edge of the surfactant front. Previous work has debated whether the surfactant front travels near the Marangoni ridge for a deposited insoluble surfactant when no predeposited surfactant is present[40] or behind the Marangoni ridge.[41] Previous work has also found that the talc tracer particles are set in motion by the surface tangential flow as the Marangoni ridge passes the particle.[29] Therefore, for the case of no predeposited surfactant, we infer that the innermost talc particles discussed above trace the deposited surfactant front.

As predicted theoretically (see Figure 1 of ref 17), the Marangoni ridge seen in this study grows in height above the baseline at early times and becomes constant in height at later times. In the case of oleic acid spreading here, the speed of the ridge, measured according to the position of the ridge peak, is 17.2 ± 2.7 cm/s (see Figure 6 and Table 1). This is similar to speeds reported in the experimental[2,16,30,42] and theoretical[1,17,40] literature, after accounting for the different subphase viscosities and calculating dimensionless velocities via eq 2.1 of ref. 15.

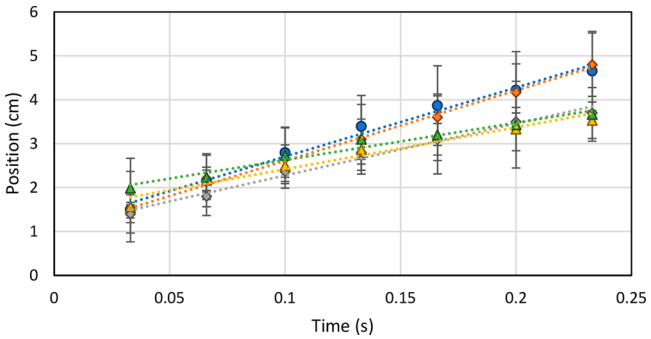

Figure 6. Position of the peak of the ridge versus time after oleic acid deposition. The initial areas of predeposited DPPC are as follows: No DPPC (blue circle), 200 (orange diamond), 134 (gray diamond), 80 (yellow triangle), 67 Å^2/molecule (green triangle). The Marangoni ridge speed and error from a linear least-squares fit for each concentration are in Table 1. For the 67 Å^2 case, there is no Marangoni ridge but the leading region of the central depression is shown and propagates at the same speed (8.6 ± 3.7 cm/s) as the ridge calculated for an initial predeposited DPPC concentration of 80 Å^2/molecule. The uncertainties are the standard deviation from multiple runs and are dominated by run to run differences. A linear fit was chosen since systematic deviations from a linear fit are undetectable within the uncertainties of the data. No slowing down of the ridge with time is detectable.

Figure 7A shows the time at which talc particles at various radial distances from the oleic acid deposition point begin to move in comparison to the Marangoni ridge peak, thus indicating the separation between the region in the subphase where there is tangential fluid movement (smaller distances) and the region where there is no detectable tangential fluid (larger distances). In panel A, the Marangoni ridge is marked by green diamonds, and the onset time of motion of tracer particles by orange squares. When no predeposited surfactant is present, there is no motion ahead of the Marangoni ridge. For example, for a particle initially at 3.2 cm, the onset time is 166 ms. At 166 ms, the peak of the Marangoni ridge is located at 3.2 cm. As suggested by modeling,[15] the data shows that for no predeposited surfactant there is little or no tangential fluid movement at the subphase surface ahead of the leading region of the Marangoni ridge peak: the onset of tracer particle motion coincides with the arrival of the Marangoni ridge peak.

Figure 8A shows a schematic created from the data in Figure 7A summarizing the spatial positions of critical features of the surface tension gradient, surface distortion, and velocity fields midway through a spreading event without predeposited surfactant. The existence of a tangential velocity only in the region where the deposited oleic acid resides and nowhere beyond that region suggests that the surface tension gradient exists within the oleic acid monolayer to a point just beyond the peak of the Marangoni ridge but not beyond the leading region of the Marangoni ridge. Beyond the Marangoni ridge, there is no detectable tangential surface velocity. The existence of the ridge indicates a vertical velocity, and therefore a normal velocity of the surface.

At about 250 ms, the Marangoni ridge hits the wall of the container, and a wave is reflected back. This time marks the end of our detailed analysis of the spreading. Over a time scale of one second, all fluid motion ceases. At this time, droplets of oleic acid can be seen in the central region of the Petri dish in equilibrium with the deposited oleic acid monolayer.

Spreading with Predeposited Surfactant. In this study, the predeposited DPPC layers span initial surface concentrations from the liquid-expanded to the liquid-expanded/liquid-condensed coexistence regime, producing initial spreading parameters, S, from 31 ± 1 to 21 ± 1 mN/m. In equilibrium, we measure the surface tension of the oleic acid monolayer to be 40.7 ± 1 mN/m. Thus, as expected, in our experiments, oleic acid did not induce spreading when the predeposited DPPC monolayer surface tension was 40 mN/m or less.

However, could the predeposited surfactant have been compressed by a spreading drop of oleic acid rather than a monolayer? To examine this possibility, we must examine the spreading coefficient, $S_{coeff} = \sigma_{subphase/air} - \sigma_{subphase/drop} - \sigma_{drop/air}$.[43] The spreading coefficient is used here to determine whether the oleic acid will spread as a bulk liquid film on the DPPC-decorated aqueous subphase, as opposed to spreading as an oleic acid monolayer. When the spreading coefficient is less than or equal to zero, spreading as bulk film does not occur. The surface tension of bulk oleic acid drop against air is 32 mN/m.[29] As noted above, oleic acid caused spreading on DPPC-decorated subphases with initial surface tensions above 40 mN/m. If we assume that the bulk oleic acid is spreading on a liquid subphase with 40 mN/m or greater surface tension, the interfacial tension of the oleic acid drop against water must

https://dx.doi.org/10.1021/acs.langmuir.0c03348
Langmuir 2021, 37, 3309−3320

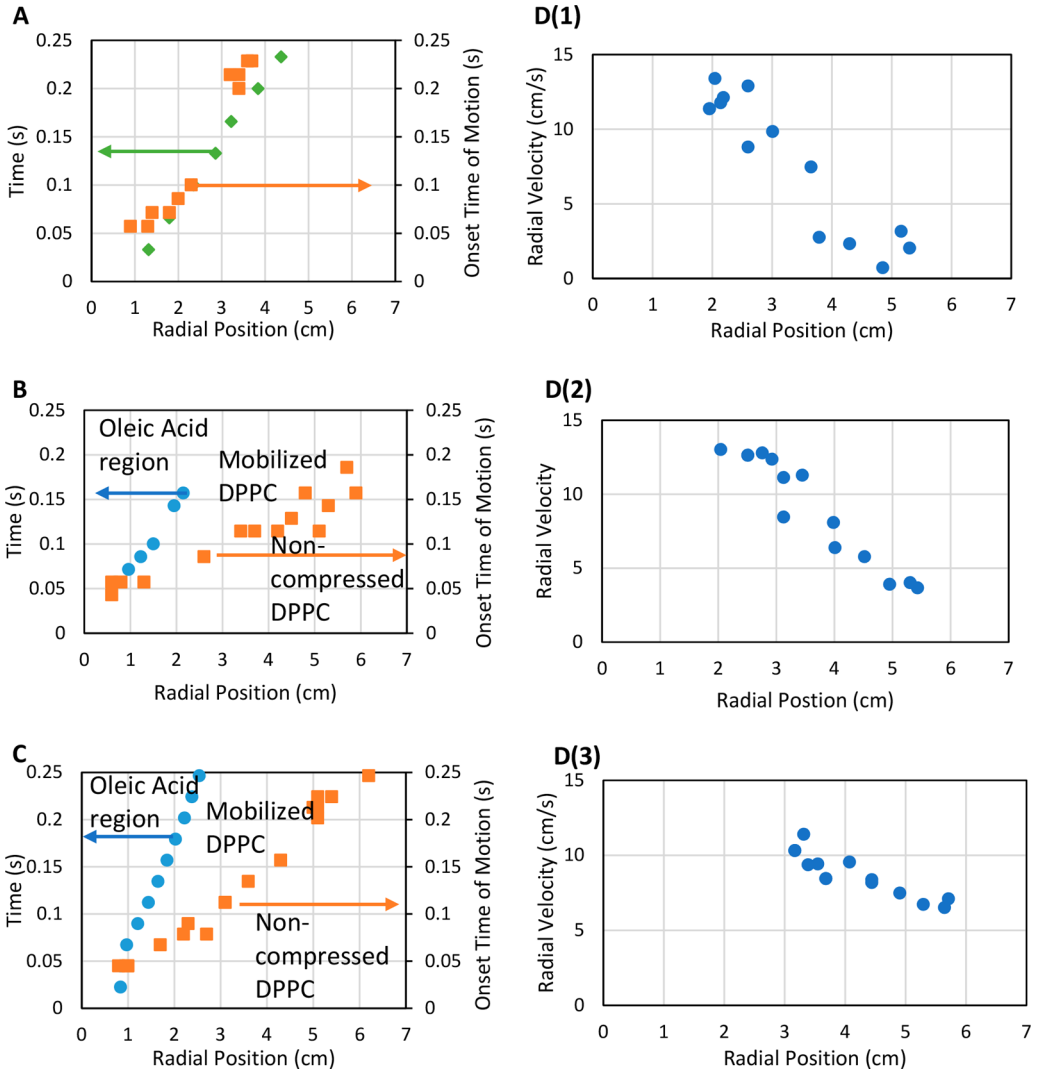

Figure 7. Measurements of tangential motion as functions of radial position. Panel A: No predeposited surfactant. (Green diamond) Time Marangoni ridge arrives at specific radial position. (orange square) time at onset of motion of tracer particle at specific radial position. Panel B: Predeposited surfactant compressed from an initial 134 Å^2/molecule. (Blue circle) Time deposited/pre deposited surfactant boundary arrives at specific radial position. (Orange square) Time at onset of motion of particle at specific radial position. Speed of outermost propagation is 42.1 ± 0.6 cm/s. Panel C: Same as panel B for predeposited surfactant compressed from an initial 67 Å^2/molecule. Speed of outermost moving particle is 23.7 ± 0.3 cm/s. Panel D: Velocity versus position for initial DPPC concentration of 134 Å^2/molecule at different times. The times are 143 (1), 186 (2), and 240 ms (3). The estimated uncertainty in positions is 0.2 cm.

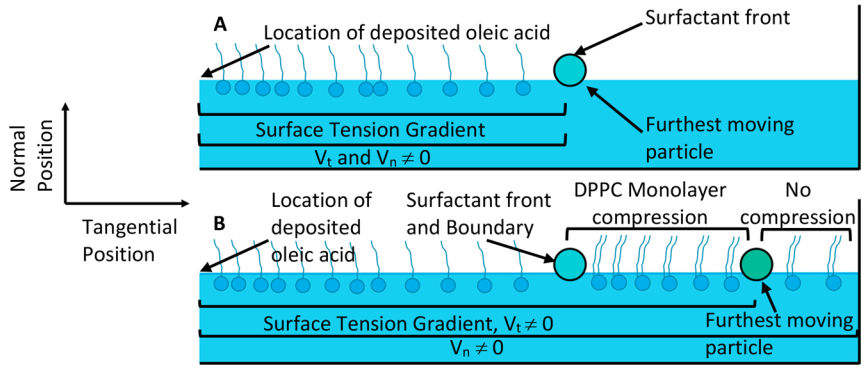

Figure 8. Schematic of spreading at a fixed time. Regions with nonzero velocity components in the normal and tangential directions are indicated. Panel A: No predeposited DPPC. Panel B: Predeposited DPPC. There is a normal component of velocity ahead of the tangential motion in the case with a moderate initial concentration of predeposited DPPC, unlike in the case with no predeposited surfactant. Also, the regions of surface tension gradients are labeled. Due to the compression of the predeposited DPPC, the surface tension gradient extends into the predeposited DPPC monolayer.

https://dx.doi.org/10.1021/acs.langmuir.0c03348
Langmuir 2021, 37, 3309−3320

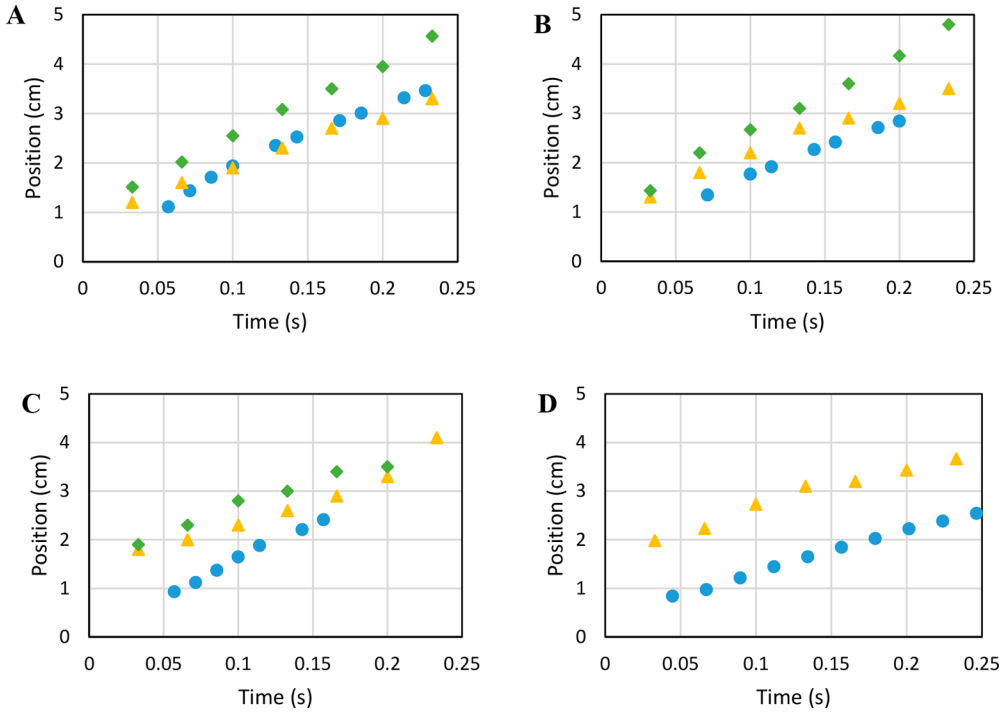

Figure 9. Relative positions of the boundary between deposited and predeposited surfactants, marked by the innermost tracer particle (circle), the peak of the Marangoni ridge (diamond), and the trailing edge of the Marangoni ridge (triangle). Panel A is for no predeposited surfactant. Panels B–D are for predeposited surfactant of concentrations of 200, 134, and 67 Å^2/molecule, respectively. The Marangoni ridge and the surfactant front are not located at the same position, yet they have similar speeds. The estimated uncertainty in the boundary is ±0.2 cm. The estimated uncertainty in the Marangoni ridge and the trailing edge locations is ±0.3 cm.

be no greater than 8 mN/m. The interfacial tensionfor oleic acid/water reported in the literature, 16.1 mN/m,[29] is significantly greater than the maximum value of 8 mN/m that would allow the spreading of a bulk oleic acid film. Therefore, the spreading examined in this paper is driven by the monolayer of oleic acid emitted by the drop and not by spreading of the oleic acid drop itself.

If the surface tension of the predeposited monolayer before spreading is greater than that of the oleic acid monoayer emitted by the deposited drops, rapid Marangoni spreading occurs due to the surface tension difference between the deposited oleic acid monolayer and the predeposited DPPC monolayer as well as any surface tension gradients within each monolayer. Figure 5B–D shows the evolution of surface deformation following the deposition of the oleic acid drop for three representative initial surface concentrations of predeposited DPPC. During the 233 ms duration over which spreading was monitored before the Marangoni ridge would hit the Petri dish wall, the predeposited DPPC monolayers were compressed from an initial average area to some average intermediate area since spreading had not concluded. For the initial average DPPC concentration of 200 Å^2/molecule, the DPPC compressed to an area of 140 Å^2/molecule in 233 ms. For the initial average DPPC concentration of 134 Å^2/molecule, the DPPC was compressed to an average area of 111 Å^2/molecule in 233 ms. Lastly, for the initial average DPPC concentration of 67 Å^2/molecule, the DPPC was compressed to an average area of 62 Å^2/molecule. (In the remainder of the paper, only the initial area per molecule will be given when discussing a specific spreading experiment.)

At the lowest surface concentration of predeposited DPPC shown (200 Å^2/molecule, Figure 5B), the Marangoni ridge remains well-defined with little change in the temporal evolution of the ridge height compared with the no predeposited surfactant case. However, the surface deformation shows a finite accumulation of fluid ahead of the ridge, in contrast to the no predeposited surfactant case where no such accumulation is detectable. We define this rise in surface height above the baseline ahead of the Marangoni ridge as the leading region excess. It is present at all times during the spreading event and is a reproducible feature of spreading against a predeposited DPPC monolayer, independent of the concentration. For example, as shown in Figure 5A, at 133 ms, there is no significant leading region excess in the absence of predeposited surfactant. The average rise above the undisturbed fluid height for the no predeposited case is 0.004 ± 0.030 mm. For the predeposited surfactant cases at the same time (Figure 5B–D), the average rise above the undisturbed fluid height for 200, 134, and 67 Å^2/molecule are 0.078 ± 0.010, 0.041 ± 0.013, and 0.109 ± 0.054 mm, respectively. The uncertainties here are dominated by the run to run variations.

The occurrence of the leading region excess indicates that a normal component of the velocity field has developed ahead of the ridge. As the concentration of predeposited surfactant increases to 134 Å^2/molecule (Figure 5C), the Marangoni ridge widens; and the maximum ridge height decreases slightly. The surface ahead of the ridge is again above the undisturbed fluid height baseline. At the most concentrated initial predeposited DPPC surface concentration (67 Å^2/molecule, Figure 5D), the Marangoni ridge is undefined, and no clear peak can be found in the height data or as a zero in the first derivative of the data. From the evolution of the height profile, it is evident that the presence of a predeposited DPPC monolayer significantly alters the overall Marangoni flow and

https://dx.doi.org/10.1021/acs.langmuir.0c03348
Langmuir 2021, 37, 3309–3320

that the alteration is more severe as the initial surface concentration of the predeposited monolayer is increased. When a Marangoni ridge forms, the fluid that produces the ridge comes from the central depression region. With predeposited DPPC at 67 Å^2/molecule, the surface tension gradient driven flow has not created a well-formed ridge from the fluid coming from the depression region. Rather, the fluid has spread outward to form a general rise of excess fluid above the undisturbed fluid height at all times analyzed. It is important to note that a leading region excess is present even when the ridge does not form. The leading region excess occurs with any concentration of predeposited surfactant, while the ridge destruction occurs only with the highest initial concentration of predeposited surfactant. The Marangoni ridge that normally forms when there is a sharp end to the deposited surfactant concentration profile[1] has been destroyed. As will be discussed below, this is likely caused by the propagation of surface tension gradients beyond the deposited surfactant front and into the predeposited DPPC monolayer.

The speed of the Marangoni ridge is dependent on the initial surface concentration of predeposited DPPC. (See Table 1.) Experiments with the initial predeposited DPPC monolayer at 200 Å^2/molecule have the same ridge speed, within error, as when there is no predeposited surfactant, as seen in Figure 6 and Table 1, with a speed of 16.3 ± 2.5 cm/s for 200 Å^2/molecule and 17.2 ± 2.7 cm/s for no predeposited DPPC. When the initial predeposited DPPC surface concentration is 134 and 80 Å^2/molecule, the ridge speed slowed down to 10.3 ± 1.2 and 8.7 ± 3.0 cm/s, respectively. At the highest initial surface concentration of predeposited DPPC, 67 Å^2/molecule, where the Marangoni ridge has been destroyed, we must take a different measure of the propagation. In this case, we measure the speed at which the outer edge of the depression (identified as the "trailing edge" in Figure 1) propagated (8.6 ± 3.7 cm/s). This speed is indistinguishable from the speed that the Marangoni ridge displayed at 80 Å^2/molecule (see Figure 6 and Table 1). The spreading parameter for initial DPPC concentration of 67 Å^2/molecule is not the same as for 80 Å^2/molecule, where the spreading parameter is 25 and 21 mN/m, respectively. This is qualitatively consistent with scaling arguments that predict the spreading speed should scale linearly with the spreading parameter.[15] We find our data consistent with previous work even though our range of the spreading parameter is narrower.[23]

For the no predeposited DPPC case, the deposited surfactant front represents the boundary between the surface tension gradient that exists within the deposited oleic acid monolayer and the constant surface tension region of the clean subphase surface. As shown in Figure 9A in this case, the surfactant front travels just behind the Marangoni ridge. For the case where the predeposited surfactant is present, the deposited surfactant front now represents the boundary between the deposited and predeposited surfactant. As will be shown below, the surface tension gradient now extends from the deposited surfactant region into the predeposited surfactant annulus and causes motion in the annulus. The boundary between the deposited and predeposited surfactant is now somewhere within the surface tension gradient which extends across the entire surface covered by either deposited or predeposited surfactant. As shown in Figures 9B–D, the boundary between oleic acid and predeposited DPPC monolayers remains behind the Marangoni ridge.

Using the talc markers, we determine the region of the predeposited DPPC annulus that is under compression as the spreading event progresses. As discussed above, the innermost talc particles mark the oleic acid/DPPC boundary during the spreading event, which can be seen in Figure 7 B and C and in Figure 9 as blue circles. The data in Figure 7 B and C show not only the position of the oleic acid/DPPC boundary as a function of time, but also the position of the outermost moving talc particle at different times. In Panel B, the boundary between the deposited oleic acid and the predeposited DPPC is marked by blue circles, and the onset time of particle motion is marked by orange squares. The onset motion data uses the right y axis, while the boundary uses the left y axis. For a particle initially at 3.4 cm, the onset time is 110 ms. At 110 ms, the deposited surfactant front is located at 1.5 cm. Hence, there is motion ahead of the boundary. Panel C can be read in a similar fashion. Again, there is motion ahead of the boundary. The Marangoni ridge and the trailing edge are not shown in Figure 7B,C.

The outermost moving particle marks the outer boundary of the mobilized DPPC region. For radial positions beyond the outermost moving tracer particle, there is no radial motion in the surface. As mentioned previously, this position is far ahead of the oleic acid/DPPC boundary. The outer boundary of the mobilized DPPC region is also moving faster than the oleic acid/DPPC boundary itself. As seen in Figure 9B,C, the boundary is approximately 0.5−1 cm behind the Marangoni ridge, while the outermost moving particle is around 1−2 cm ahead of the boundary, as seen in Figure 7B. This signifies that, when a Marangoni ridge is present, there is motion ahead of both the Marangoni ridge and the deposited surfactant front. In Figure 9D (67 Å^2/molecule), for which there is no discernible Marangoni ridge peak, the boundary is approximately 1 cm behind the trailing edge of the surface distortion.

As seen in Figures 6 and 7, the ridge speed was on the order of 10 cm/s, and the speed of the outer mobilized DPPC boundary was 42.1 ± 0.6 cm/s, for 134 Å^2/molecule. As seen in Figure 9, the slopes for the Marangoni ridge peak position and the surfactant front are the same, signifying that the surfactant front moves at the same speed as the Marangoni ridge, even though they are not located in the same position. For 67 Å^2/molecule, where there was no Marangoni ridge peak, the trailing edge speed was again on the order of 10 cm/s and the speed of the outer mobilized DPPC boundary was 23.7 ± 0.3 cm/s. Our observation that the propagation of the outer boundary at a faster speed than the Marangoni ridge is consistent with other experimental systems, as seen in Bull et al.[17,22] Thus, in cases with predeposited DPPC monolayers, there is a significant tangential movement of the surface ahead of both the oleic acid/DPPC boundary and the Marangoni ridge when a well-formed ridge is present (200, 134 Å^2) or ahead of the oleic acid/DPPC boundary and trailing edge when no ridge is present (67 Å^2).

The data in Figure 7 reveal how the inner and outer limits of the annular compression region of mobilized DPPC change with time. The outer boundary moves outward faster than the inner limit, showing that the compressed annulus broadens with time. The predeposited DPPC is being compressed at rates of ∼100 Å^2 molecule^{-1} min^{-1} at high surface concentrations of predeposited DPPC and at ∼1000 Å^2 molecule^{-1} min^{-1} at low concentrations of predeposited DPPC averaged across the annulus. We note that these compression rates are two to 3 orders of magnitude greater

https://dx.doi.org/10.1021/acs.langmuir.0c03348
Langmuir 2021, 37, 3309−3320

than the rates imposed in typical Langmuir trough measurements of lipid monolayer surface pressure isotherms,[44] which are generally on the order of ~2 Å^2 molecule^{-1} min^{-1}. This brings into question the suitability of considering Marangoni spreading as being dictated by the equilibrium isotherm. Even at the much more modest rates of a Langmuir trough experiment, the surface pressure isotherms of DPPC deviate from the equilibrium isotherm to an extent that increases with increasing compression rate.[25]

In Figure 7, it is shown clearly that there is nonuniform compression of predeposited DPPC outside the oleic acid/DPPC boundary due to the fact that not the entire annulus of DPPC is mobilized. Furthermore, the velocities within the mobilized DPPC region decrease as r increases, as shown for various instants of time in Figure 7D.

Figure 8 B shows a schematic created from the data in Figure 7B,C, summarizing the spatial positions of critical features of the surface tension gradients, surface distortion and velocity fields midway through the spreading event with predeposited surfactant. The surface tension gradient extends from the oleic acid monolayer, through the deposited/predeposited surfactant boundary to the point where the there is no detectable movement of the tracer particles. This is in contrast to the no predeposited surfactant case, where there is no tangential velocity ahead of the Marangoni ridge, i.e., beyond the furthest moving tracer particle (Figure 7A). In the case with predeposited surfactant, motion occurs well ahead of the oleic acid/DPPC boundary because the surface tension gradient extends ahead of the Marangoni ridge and drives the flow in that region. Beyond that mobilized DPPC region, which is expanding outward at a speed faster than the Marangoni ridge moves outward, there is no detectable tangential surface velocity, but there is fluid velocity normal to the surface as evidenced by the surface deformation that was observed well ahead of the Marangoni ridge, as seen with all predeposited DPPC cases. This normal velocity may be driven by subsurface flows at smaller radial positions or by the flow impinging on the wall of the dish or a combination of both.

The nonuniform compression of the predeposited surfactant leads to a finite surface tension gradient beyond the advancing oleic acid/DPPC boundary. For the case with no predeposited surfactant, there may be a surface tension gradient in the monolayer of the advancing deposited surfactant; but ahead of the advancing deposited surfactant front, there is a constant surface tension equal to that of the bare surface which is higher than the surface tension of the advancing deposited surfactant. For the case of predeposited surfactant, there may be a surface tension gradient in the monolayer of deposited surfactant. This surface tension gradient joins at the deposited/predeposited surfactant boundary to the surface tension gradient created in the mobilized inner part of the predeposited annulus. The surface tension gradient in the mobilized portion of the annulus is at least partially responsible for the fluid motion seen ahead of the Marangoni ridge and the deposited/predeposited surfactant boundary. At earlier times, the gradient ends at the outer boundary of the mobilized annulus. At later times, around 0.4 s, the surface tension gradient in the entire predeposited annulus extends to the boundary of the dish and evolves. This is more than 0.15 s after the last frame shown for surface height deformation.

End of Spreading. At about 1 s, when all motion has ceased, the system returns to a state of mechanical equilibrium, suggesting that the two unmixed monolayers must have the same surface tension. Within the centrally located deposited oleic acid monolayer, droplets of oleic acid formed by autophobing of the oleic acid[29] were seen in equilibrium with the oleic acid monolayer. In equilibrium, we measure the surface tension of the oleic acid monolayer to be 40.7 ± 1 mN/m. We measured the surface tension in the predeposited DPPC region after the oleic acid spreading was completed to be 40.4 ± 4.1 mN/m, independent of the initial predeposited DPPC surface concentration before spreading. Thus, when motion ends, there is a surface pressure balance between the two regions of unmixed monolayers, as required for mechanical equilibrium. This further suggests that even the very rapid fluid motion during the spreading event does not cause mixing between the oleic acid and DPPC as initially found in fluorescence microscopy (see Figure 2). As further evidence of a lack of mixing of the monolayers, we monitored the surface using fluorescence microscopy for 15 min after spreading and saw no broadening of the boundary between the monolayers.

The final area per DPPC molecule in the compressed monolayer annulus was calculated from the known total amount of DPPC deposited and the final annulus area. In all cases it was 41.6 ± 3.4 Å^2/molecule, which matches the equilibrium area per molecule expected for the 40.4 ± 4.1 mN/m measured final surface tension based on the DPPC surface tension isotherm. So while the equilibrium equation of state cannot hold during the rapid compression of the predeposited monolayer, the cessation of spreading is nevertheless dictated by equilibrium mechanics as established by the equilibrium equation of state for DPPC. Had there been intermixing of oleic acid and DPPC, or had there been collapse of the DPPC monolayer, we would not have obtained the correct area per DPPC molecule based on the final surface tension of the DPPC monolayer. This further bolsters our evidence that there is no significant surfactant intermixing on the time scale of the experiments. It also supports the argument, based on the lack of dark ridges in the fluorescence microscope images, that there is no DPPC monolayer collapse in the compressed annulus. Even with the rapid compression rates generated by oleic acid spreading, the DPPC monolayer was not compressed to collapse. Had the monolayer collapsed, which is a condition of infinite compressibility, it would have not provided the observed resistance to stop the spreading.

CONCLUSIONS

The presence of a pre-existing insoluble surfactant monolayer fundamentally alters Marangoni spreading events relative to spreading on an initially clean surface. Spreading occurs as long as the surface tension of the deposited surfactant monolayer is less than that of the predeposited monolayer. At all values of the initial spreading parameter, the compression of the predeposited surfactant is nonuniform ahead of the deposited surfactant/predeposited surfactant boundary. As spreading progresses, a surface tension gradient evolves from the deposited surfactant monolayer through the boundary between the deposited surfactant/predeposited surfactant. At early times, only the inner portion of the annulus of predeposited surfactant is mobilized. The outer boundary of that mobilized region moves outward at a speed greater than the propagation speed of the Marangoni ridge. All motion ceases when the surface concentration in the predeposited annulus becomes uniform with a surface tension equal to that of the deposited surfactant monolayer.

https://dx.doi.org/10.1021/acs.langmuir.0c03348
Langmuir 2021, 37, 3309−3320

The surface tension gradient that propagates beyond the deposited surfactant/predeposited surfactant boundary produces Marangoni stresses that drive flows both tangential and normal to the subphase surface. At an initial spreading parameter of 31 mN/m, the surface tension gradient is steep enough in the vicinity of the deposited/predeposited surfactant boundary that the shock-like Marangoni ridge still develops as it normally would for Marangoni spreading with no predeposited surfactant. The Marangoni ridge moves at the same speed in the two cases. However, in contrast to spreading on an initially clean subphase, the Marangoni stresses that cause flow tangential and normal to the surface ahead of the Marangoni ridge in the predeposited surfactant annulus distort the surface well ahead of the Marangoni ridge. For an initial spreading parameter of 21.4 mN/m, the gradient is not sufficiently steep to drive a shock-like Marangoni ridge even though fluid is strongly transported away from the point of surfactant deposition. Instead of a well-formed ridge, there is a broad region of elevated surface height above the initial undisturbed fluid level.

This work addresses important questions in applications when Marangoni spreading occurs in the presence of pre-existing of surfactants or other surface active materials, such as in oil spill cleanup and pulmonary drug delivery. The results of this study suggest that spreading induced by deposition of an exogenous surfactant is possible in the presence of an endogenous surfactant in the lung, as long as the surface tension of the deposited surfactant is lower than that of the predeposited material. Thus, exogenous surfactant could aid pulmonary drug delivery even though at least some portions of the lung airway are coated with endogenous lipid.[17,22,45] Similarly, surfactant deposited around an oil spill may be expected to corral the spilled oil as long as the deposited surfactant has a lower surface tension than the spilled oil, but the degree of such corralling may be limited if the surface tension of the pre-existing material increases as it is compressed by the applied surfactant.

From a fundamental standpoint, this study probes how predeposited insoluble surfactant changes the current understanding of how the Marangoni spreading in the presence of predeposited surfactant varies from the case without predeposited surfactant. This work is consistent with prior studies of the effect of predeposited surfactant on the speed of Marangoni spreading induced by insoluble surfactant, and it shows for the first time how predeposited surfactant monolayers distort or eliminate the Marangoni ridge. The deposited oleic acid and predeposited DPPC monolayers do not mix during the very rapid spreading event. The speed of the compression of the predeposited DPPC makes it unlikely that equilibrium equations of state can describe the evolution of the surface tension during its compression. The proper way to account for a dynamic equation of state should be a subject for future work.

To further the work applied to pulmonary drug delivery, future fundamental work needs to focus on spreading on thin, chemically complex subphases. In the lung, the endogenous phospholipids are on top of a complex thin mucus subphase. Mucus is a complex solution of lipids, ions, and glycoproteins in water and has complex rheology.[46] Thus, the development of Marangoni stresses on the lung airway will depend on the bulk and surface composition of the mucus. Further, since the mucus layer in the lung is thin, dewetting of the mucus from the underlying periciliary layer may occur.[15,18,47] The impact of endogenous lipid on that dewetting process has not been explored.

AUTHOR INFORMATION

Corresponding Authors

Robert D. Tilton − *Center for Complex Fluids Engineering, Department of Chemical Engineering, and Department of Biomedical Engineering, Carnegie Mellon University, Pittsburgh, Pennsylvania 15213, United States;* orcid.org/0000-0002-6535-9415; Email: tilton@cmu.edu

Stephen Garoff − *Department of Physics and Center for Complex Fluids Engineering, Carnegie Mellon University, Pittsburgh, Pennsylvania 15213, United States;* Email: sg2e@andrew.cmu.edu

Authors

Madeline L. Sauleda − *Department of Physics and Center for Complex Fluids Engineering, Carnegie Mellon University, Pittsburgh, Pennsylvania 15213, United States;* orcid.org/0000-0001-8753-2154

Henry C. W. Chu − *Center for Complex Fluids Engineering and Department of Chemical Engineering, Carnegie Mellon University, Pittsburgh, Pennsylvania 15213, United States; Department of Chemical Engineering, University of Florida, Gainesville, Florida 32611, United States*

Complete contact information is available at: https://pubs.acs.org/10.1021/acs.langmuir.0c03348

Notes

The authors declare no competing financial interest.

ACKNOWLEDGMENTS

We thank Boyan Yin for her invaluable help with spreading experiments. This work was funded by the National Science foundation under Grants NSF-CBET- 1510293 and NSF-CBET 1921285. H.C.W. Chu acknowledges the startup funding support from the Division of Sponsored Programs, Department of Chemical Engineering, and Herbert Wertheim College of Engineering at University of Florida.

REFERENCES

(1) Craster, R. V.; Matar, O. K. Dynamics and stability of thin liquid film. *Rev. Mod. Phys.* **2009**, *81* (3), 1131−1198.

(2) Afsar-Siddiqui, A. B.; Luckham, P. F.; Matar, O. K. The spreading of surfactant solutions on thin liquid films. *Adv. Colloid Interface Sci.* **2003**, *106*, 183−236.

(3) Grotberg, J. B. Respiratory fluid mechanics and transport processes. *Annu. Rev. Biomed. Eng.* **2001**, *3*, 421−457.

(4) Levy, R.; Hill, D. B.; Forest, M. G.; Grotberg, J. B. Pulmonary Fluid Flow Challenges for Experimental and Mathematical Modeling. *Integr. Comp. Biol.* **2014**, *54* (6), 985−1000.

(5) Evans, P.L.; Schwartz, L.W.; Roy, R.V. A mathematical model for crater defect formation in a drying paint layer. *J. Colloid Interface Sci.* **2000**, *227*, 191−205.

(6) La Due, J.; Muller, M. R.; Swangler, M. Cratering phenomena on aircraft anti-icing films. *J. Aircr.* **1996**, *33*, 131−138.

(7) Gupta, D.; Sarker, B.; Thadikaran, K.; John, V.; Maldarelli, C.; John, G. Sacrificial amphiphiles: Eco-friendly chemical herders as oil spill mitigation chemicals. *Sci. Adv.* **2015**, *1*, 1−6.

(8) Espinosa, F. F.; Shapiro, A. H.; Fredberg, J. J.; Kamm, R. D. Spreading of exogenous surfactant in an airway. *J. Appl. Physiol.* **1993**, *75* (5), 2028−2039.

(9) Waters, S. L.; Grotberg, J. B. The propagation of a surfactant laden liquid plug in a capillary tube. *Phys. Fluids* **2001**, *12*, 471.

(10) Iasella, S. V.; Stetten, A. Z.; Corcoran, T. E.; Garoff, S.; Przybycien, T. M.; Tilton, R. D. Aerosolizing lipid dispersions enables antibiotic transport across mimics of the lung airway surface even in the presence of pre-existing lipid monolayers. *J. Aerosol Med. Pulm. Drug Delivery* **2018**, *31* (4), 212−220.
(11) Stetten, A. Z.; Moraca, G.; Corcoran, T. E.; Tristram-Nagle, S.; Garoff, S.; Przybycien, T. M.; Tilton, R. D. Enabling Marangoni flow at air-liquid interfaces through deposition of aerosolized lipid dispersions. *J. Colloid Interface Sci.* **2016**, *484*, 270−278.
(12) Gaver, D. P.; Grotberg, J. B. Droplet spreading on a thin viscous film. *J. Fluid Mech.* **1992**, *235*, 399−414.
(13) Halpern, D.; Jensen, O. E.; Grotberg, J. B. A Theoretical study of surfactant and liquid delivery into the lung. *J. Appl. Physiol.* **1998**, *85*, 333−352.
(14) Halpern, D.; Fujioka, H.; Takayama, S.; Grotberg, J. B. Liquid and surfactant delivery into pulmonary airways. *Respir. Physiol. Neurobiol.* **2008**, *163*, 222−231.
(15) Gaver, D. P.; Grotberg, J. B. The dynamics of a localized surfactant on a thin film. *J. Fluid Mech.* **1990**, *213*, 127−147.
(16) Iasella, S. V.; Sun, N.; Zhang, X.; Corcoran, T. E.; Garoff, S.; Przybycien, T. M.; Tilton, R. D. Flow regime transitions and effects on solute transport in surfactant-driven Marangoni flows. *J. Colloid Interface Sci.* **2019**, *553*, 136−147.
(17) Grotberg, J. B.; Halpern, D.; Jensen, O. E. Interaction of exogenous and endogenous surfactant: spreading-rate effects. *J. Appl. Physiol.* **1995**, *78* (2), 750−756.
(18) Tsai, W. T.; Liu, L. Y. Transport of exogenous surfactants on a thin viscous film within an axisymmetric airway. *Colloids Surf., A* **2004**, *234* (1), 51−62.
(19) Williams, H. A. R.; Jensen, O. E. Surfactant transport over airway liquid lining of nonuniform depth. *J. Biomech. Eng.* **2000**, *122* (2), 159−165.
(20) Cassidy, K. J.; Halpern, D.; Ressler, B. G.; Grotberg, J. B. Surfactant effects in model airway closure experiments. *J. Appl. Physiol.* **1999**, *87*, 415−427.
(21) Espinosa, F. F.; Kamm, R. D. Bolus dispersal through the lungs in surfactant replacement therapy. *J. Appl. Physiol.* **1999**, *86* (1), 391−410.
(22) Bull, J. L.; Nelson, L. K.; Walsh, J. T.; Glucksberg, M. R.; Schurch, S.; Grotberg, J. B. Surfactant-spreading and surface-compression disturbance on a thin viscous film. *J. Biomech. Eng.* **1999**, *121* (1), 89−98.
(23) Bull, J. L.; Grotberg, J. B. Surfactant spreading on thin viscous films: film thickness evolution and periodic wall stretch. *Exp. Fluids* **2003**, *34* (1), 1−15.
(24) Schenck, D.; Goettler, S.; Fiegel, J. Surfactant-induced spreading of nanoparticles is inhibited on mucus mimetic surfaces that model native lung conditions. *Phys. Biol.* **2019**, *16* (6), 065001.
(25) Duncan, S. L.; Larson, R. G. Comparing experimental and simulated pressure-area isotherms for DPPC. *Biophys. J.* **2008**, *94* (8), 2965−2986.
(26) NIST/SEMATECH e-Handbook of Statistical Methods, http://www.itl.nist.gov/div898/handbook/, 2013.
(27) Fuchs, N. A. *The mechanics of aerosols*; Dover Publications, 1989; pp 154−155.
(28) Rasband, W. S. *ImageJ*; U. S. National Institutes of Health: Bethesda, MD, 1997−2018; https://imagej.nih.gov/ij/.
(29) Sharma, R.; Kalita, R.; Swanson, E.; Corcoran, T. E.; Garoff, S.; Przybycien, T. M.; Tilton, R. D. Autophobing on liquid subphases driven by the interfacial transport of amphiphilic molecules. *Langmuir* **2012**, *28*, 15212−15221.
(30) Wang, X.; Bonaccurso, E.; Venzmer, J.; Garoff, S. Deposition of drops containing surfactants on liquid pools: Movement of the contact line, Marangoni ridge, capillary waves and interfacial particles. *Colloids Surf., A* **2015**, *486*, 53−59.
(31) Lewis, D.; Hadgraft, J. Mixed monolayers of dipalitoylphosphatidylcholine with Azone or oleic acid at the air-water interface, I. *J. Pharma.* **1990**, *65*, 211−218.
(32) Kurniawan, J.; Suga, K.; Kuhl, T. L. Interaction forces and membrane charge tuneability: Oleic acid containing membranes in different pH conditions. *Biochim. Biophys. Acta, Biomembr.* **2017**, *1859*, 211−217.
(33) Notman, R.; Noro, M. G.; Anwar, J. Interaction of oleic acid with dipalmitoylphosphatidylcholine (DPPC) bilayers simulated by molecular dynamics. *J. Phys. Chem. B* **2007**, *111* (44), 12748−12755.
(34) Goncalves da Silva, A. M.; Romao, R. I. S. Mixed monolayers involving DPPC, DODAB, and oleic acid and their interaction with nicotinic acid and the air-water interface. *Chem. Phys. Lipids* **2005**, *137*, 62−76.
(35) Busquets, M. A.; Mestres, C.; Alsina, M. A.; Garcia Anton, J. M.; Reig, F. Miscibility of dipalitoylphosphatidylcholine, oleic acid and cholesterol measured by DSC and compression isotherms of monolayers. *Thermochim. Acta* **1994**, *232*, 261−269.
(36) Ybert, C.; Lu, W.; Moller, G.; Knobler, C. M. Collapse of a Monolayer by Three Mechanisms. *J. Phys. Chem. B* **2002**, *106*, 2004−2008.
(37) Oppenheimer, N.; Diamant, H.; Witten, T. A. Anomalously fast kinetics of lipid monolayer buckling. *Phys. Rev. E* **2013**, *88* (2), 022405.
(38) Lipp, M. M.; Lee, K. Y. C.; Takamoto, D. Y.; Zasadzinski, J. A.; Waring, A. J. Coexistence of buckled and flat monolayers. *Phys. Rev. Lett.* **1998**, *81* (8), 1650−1653.
(39) Baoukina, S.; Monticelli, L.; Risselada, H. J.; Marrink, S. J.; Tieleman, D. P. The molecular mechanism of lipid monolayer collapse. *Proc. Natl. Acad. Sci. U. S. A.* **2008**, *105*, 10803−10808.
(40) Fallest, D. W.; Lichtenberger, A. M.; Fox, C. J.; Daniels, K. E. Fluorescent visualization of a spreading surfactant. *New J. Phys.* **2010**, *12* (7), 073029.
(41) Sharma, R.; Corcoran, T. E.; Garoff, S.; Przybycien, T. M.; Tilton, R. D. Transport of a partially wetted particle at the liquid/vapor interface under the influence of an externally imposed surfactant generated Marangoni stress. *Colloids Surf., A* **2017**, *521*, 49−60.
(42) Harkins, W. D.; Feldman, A. The spreading of liquids and the spreading coefficient. *J. Am. Chem. Soc.* **1922**, *44*, 2665−2685.
(43) Charron, J. R.; Tilton, R. D. A Scanning Angle Reflectometry Investigation of Block Copolymer Adsorption to Insoluble Lipid Monolayers at the Air- Water Interface. *J. Phys. Chem.* **1996**, *100* (8), 3179−3189.
(44) Avery, M. E.; Mead, J. Surface properties in relation to atelectasis and hyaline membrane disease. *AMA J. Disease Children* **1959**, *97* (5), 517−523.
(45) Ridley, C.; Thornton, D. J. Mucins: the frontline defence of the lung. *Biochem. Soc. Trans.* **2018**, *46* (5), 1099−1106.
(46) Button, B.; Cai, L. H.; Ehre, C.; Kesimer, M.; Hill, D. B.; Sheehan, J. K.; Boucher, R. C.; Rubinstein, M. A Periciliary Brush Promotes the Lung Health by Separating the Mucus Layer from Airway Epithelia. *Science* **2012**, *337*, 937−941.
(47) Dussaud, A. D.; Matar, O. K.; Troian, S. M. Spreading characteristics of an insoluble surfactant film on a thin liquid layer: comparison between theory and experiment. *J. Fluid Mech.* **2005**, *544*, 23−51.

https://dx.doi.org/10.1021/acs.langmuir.0c03348
Langmuir 2021, 37, 3309−3320